Experimental characterization of operating bladed rotor using harmonic power spectra and stochastic subspace identification

D.Tcherniak[1], S. Yang[2], M.S. Allen [3]
[1] Brüel and Kjær Sound and Vibration Measurement
Skodsborgvej 307, Nærum 2850, Denmark
e-mail: **dtcherniak@bksv.com**

[2] Turbomachinery Systems, Praxair Inc.
175 East Park Drive, Tonawanda, NY 14150

[3] Department of Engineering Physics, University of Wisconsin-Madison
535 Engineering Research Building, 1500 Eng. Drive, Madison, WI 53706, USA

Abstract
The dynamic response of mechanical systems with rotating elements (for example, operating wind turbines) cannot be described using a classical linear time-invariant (LTI) formulation because the mass and stiffness matrices can be periodically varying while the rotor rotates. Such systems belong to the class of linear periodic time variant (LPTV) systems, which require special treatment for their experimental identification. For instance, the Harmonic Power Spectra (HPS) method, which is based on Floquet theory, can be applied. Following this method, the experimentally obtained responses are exponentially modulated using the rotational frequency, the HPS matrix is computed between the modulated responses and is used as the input to Operational Modal Analysis (OMA). The latter provides frequencies of the modes and the Fourier coefficients for reconstructing the time periodic mode shapes. In authors' prior works the HPS method has been applied in the frequency domain. The presented study extends the HPS method to the time domain, which makes it possible to use the powerful stochastic subspace identification (SSI) techniques for modal identification, which lead to more accurate parameter estimates and can treat modes with close frequencies. The advantage of the suggested approach is that it allows the use of existing implementations of SSI, thus providing a simple tool for modal identification of periodic systems.

1 Introduction

Operational modal analysis (OMA) [1], a method of extracting the modes and hence a linear dynamic model of a structure from operational measurements, has become a mainstream technology in the past few decades. Often the structures of interest involve rotating machinery (e.g., operating wind turbines), which makes the application of well-established OMA techniques invalid since the structure under test is not time invariant, and this violates the main assumption of modal analysis. If the structural properties change periodically, the structure can be modelled as a linear periodic time variant (LPTV) system. Currently the number of studies on identification of LPTV systems remains limited. Study [2] suggested using so-called Coleman (also known as multiblade coordinate, MBC) transformation as a preprocessing step to OMA. By changing variables to a rotational frame, Coleman transformation converts the LPTV system to LTI, which then allows application of wide range of classical modal identification techniques. However, this method can only be applied to isotropic rotors, i.e. when all blades have identical mass and structural properties. In addition, for rotors rotating in vertical plane, as in a case of horizontal axis wind turbines (HAWT), the gravity introduces forces that break symmetry and can cause the system to exhibit liner time periodic

behavior. This prevents using the transformation for in-plane modes. Jhinaoui [3] suggested a subspace identification method specially developed for rotating systems. The method identifies the underlying Floquet eigenstructure of the rotating system and uses the samples obtained at the same position of the rotor at consecutive revolutions. Allen suggested using harmonic power spectra (HPS) for structures identification and extended experimental modal analysis to LPTV systems [4] and later to OMA in [5]. This framework has been used quite extensively to extract the mode shapes from continuous-scan laser vibrometer measurements [6-9] and the authors recently applied it to measurements from an operating wind turbine in [10].

The first step when computing HPS is to modulate the measured time histories by multiplying them by $e^{-\mathrm{i}m\Omega t}$ where Ω is the rotation frequency of the turbine and m is some integer. Then, the theory shows that the augmented set of measurements can be processed using standard curve fitting techniques or peak picking to extract the natural frequencies and damping ratios. The theory also explains how to relate the amplitudes of the harmonics in the response to the time-varying mode shapes. The method described in [5] uses *frequency domain* modal algorithms to extract modal parameters; in this paper, we refer to this method as H-OMA-FD. The presented paper extends this technique to *time domain* OMA; the suggested approach is referred as H-OMA-TD.

The consequence of the harmonic modulation process is that it causes the modulated time series to be complex and hence not amenable to analysis by conventional OMA SSI routines. This work proposes an approach that circumvent this difficulty so that powerful and robust OMA subspace identification (SSI) algorithms can be used to extract the structure's modal parameters.

2 Theoretical background

The state space model of an N degrees of freedom linear time periodic system can be written as,

$$\begin{aligned}\dot{\mathbf{x}}(t) &= \mathbf{A}(t)\mathbf{x}(t) + \mathbf{B}(t)\mathbf{u}(t)\\ \mathbf{y}(t) &= \mathbf{C}(t)\mathbf{x}(t) + \mathbf{D}(t)\mathbf{u}(t)\end{aligned} \tag{1}$$

where $\mathbf{A}(t)$ is the system matrix, $\mathbf{B}(t)$ is the input matrix, $\mathbf{C}(t)$ is the output matrix, and $\mathbf{D}(t)$ is the direct input matrix. All these matrices are periodic with time. For example, the classical system with mass, damping and stiffness matrices $\mathbf{M}$, $\mathbf{C}_d$ and $\mathbf{K}$ with the following equation of motion,

$$\mathbf{M}(t)\ddot{\mathbf{z}}(t) + \mathbf{C}_d(t)\dot{\mathbf{z}}(t) + \mathbf{K}(t)\ddot{\mathbf{z}}(t) = \mathbf{f}(t) \tag{2}$$

can be written in this form using $\mathbf{x}(t) = [\mathbf{z}(t)^{\mathrm{T}} \quad \dot{\mathbf{z}}(t)^{\mathrm{T}}]^{\mathrm{T}}$ see [6] for further details. For any initial state and input pair $(\mathbf{x}(t_0), \mathbf{u}(t_0))$, a unique solution $\mathbf{y}(t)$ exists and can be written in terms of the state transition matrix $\mathbf{\Phi}(t, t_0)$ [12].

$$\mathbf{y}(t) = \mathbf{C}(t)\mathbf{\Phi}(t,t_0)\mathbf{x}(t_0) + \mathbf{C}(t)\int_{t_0}^{t}\mathbf{\Phi}(t,\tau)\mathbf{B}(\tau)\mathbf{u}(\tau)d\tau + \mathbf{D}(t)\mathbf{u}(t) \tag{3}$$

The general solution (with the direct input matrix $\mathbf{D}(t)$ equals zero) is the basis of the Floquet analysis and was used in [13] and [5] to derive the harmonic transfer function and HPS used in operational modal analysis.

2.1 Floquet Analysis

The state transition matrix $\mathbf{\Phi}(t, t_0)$ is the key to obtain the general solution in Eq.(3). When the system is linear time invariant, i.e., $\mathbf{A}(t)$=$\mathbf{A}$ and other coefficient matrices are constant, the state transition matrix is $e^{\mathbf{A}\times(t,t_0)}$, which can be further decomposed as,

$$\mathbf{\Phi}(t,t_0) = e^{\mathbf{A}\times(t-t_0)} = \mathbf{P}e^{\mathbf{\Lambda}\times(t-t_0)}\mathbf{P}^{-1} \tag{4}$$

where $\mathbf{P}$ is the matrix of eigenvectors of the system matrix $\mathbf{A}$ and $\mathbf{\Lambda}$ is a diagonal matrix of eigenvalues.

On the other hand, when the system is periodic, i.e., $\mathbf{A}(t) = \mathbf{A}(t+T)$, where $T = 2\pi/\Omega$ is the fundamental period, the dynamics of the periodic system has to be studied using Floquet theory [12,14-16] because $\mathbf{\Phi}(t,t_0) \neq e^{\mathbf{A}(t)\times(t,t_0)}$ The Floquet theory introduces a coordinate change to the system matrix $\mathbf{A}(t)$ and transforms the LPTV system to an LTI system. As a result, the state transition matrix becomes,

$$\mathbf{\Phi}(t,t_0) = \overline{\mathbf{P}}(t)e^{\mathbf{L}\times(t-t_0)}\overline{\mathbf{P}}(t_0)^{-1} \tag{5}$$

Here $\overline{\mathbf{P}}(t)$ is a periodic matrix. The eigenvalues of $\mathbf{L}$ are called the *Floquet exponents* [15,16] and it is important to note that they are still constant even though $\mathbf{A}(t)$ is time periodic. If all Floquet exponents are non-zero and non-repeated, i.e., $\mathbf{L}$ is nonsingular, then there exists a nonsingular matrix $\mathbf{R}$ that diagonalizes $\mathbf{L}$ with $\mathbf{L} = \mathbf{R}\mathbf{\Lambda}\mathbf{R}^{-1}$. Then, the state transition matrix in Eq.(5) becomes,

$$\mathbf{\Phi}(t,t_0) = \mathbf{P}(t)e^{\mathbf{\Lambda}\times(t-t_0)}\mathbf{P}(t_0)^{-1}. \tag{6}$$

where $\mathbf{P}(t) = \overline{\mathbf{P}}(t)\mathbf{R}$ is a matrix of time periodic eigenvectors for the LPTV system [17]. The state transition matrix can be further decomposed into the following modal summation form,

$$\mathbf{\Phi}(t,t_0) = \sum_{r=1}^{2N} \boldsymbol{\psi}_r(t)\mathbf{L}_r(t_0)e^{\lambda_r(t-t_0)}, \tag{7}$$

where $\boldsymbol{\psi}_r(t)$ is the r^{th} column of $\mathbf{P}(t)$, and $\mathbf{L}_r(t)$ is the r^{th} row of $\mathbf{P}(t)^{-1}$. λ_r is the r^{th} Floquet exponent that is analogous to the r^{th} eigenvalue of an LTI system. The r^{th} Floquet exponent can be written in terms of the damping ratio ζ_r and natural frequency ω_r as $\lambda_r = -\zeta_r\omega_r + \mathrm{i}\omega_r\sqrt{1-\zeta_r^2}$ for an underdamped mode. Thus the steady state response $\mathbf{y}(t)$ in Eq.(3) becomes,

$$\begin{aligned} \mathbf{y}(t) &= \sum_{r=1}^{n} \mathbf{R}_{y,r}(t)\, e^{\lambda_r(t-t_0)} \\ \mathbf{R}_{y,r}(t) &= \mathbf{C}(t)\boldsymbol{\psi}_r(t)\mathbf{L}_r(t_0)\mathbf{x}(t_0) \end{aligned} \tag{8}$$

The residue matrix $\mathbf{R}_{y,r}(t)$ is periodic and can be expanded in a Fourier series. Here we shall presume that the residue matrix can be adequately represented using a fixed number $2N_B+1$ of terms,

$$\mathbf{R}_{y,r}(t) = \sum_{n=-N_B}^{N_B} \mathbf{B}_{n,r}\, e^{\mathrm{i}n\Omega(t-t_0)}, \tag{9}$$

where $\mathbf{B}_{n,r}$ is the n^{th} Fourier coefficient matrix of the r^{th} mode. So, the output $\mathbf{y}(t)$ becomes,

$$\mathbf{y}(t) = \sum_{r=1}^{2N}\sum_{n=-N_B}^{N_B} \mathbf{B}_{n,r}\, e^{(\lambda_r+\mathrm{i}n\Omega)(t-t_0)}. \tag{10}$$

This equation reveals that the response of each mode of the system is a sum of damped sinusoids, with several sideband harmonics around each natural frequency.

2.2 Harmonic Transfer Function

Similar to what was shown above for the transient response, when an LPTV system is excited by a sinusoidal force at some frequency, the response will be at the same frequency and at an infinite number of its harmonics, each separated by the fundamental frequency Ω. At first glance it seems that it would be impossible to use a linear transfer function for a system such as this. However, Wereley overcame this difficulty by augmenting the input and output signals with frequency shifted copies of each and then the couplings between the frequencies can be accounted for in the augmented version [18]. Specifically, the m^{th} modulated signal is given by

$$\mathbf{y}_m(t) = \mathbf{y}(t)e^{-\mathrm{i}m\Omega t} \tag{11}$$

for $m \in \mathbb{N}, m = -M \ldots M$. The Fourier transform of each signal is denoted $\mathbf{y}_m(\omega)$. The frequency shifted copies are then collected as $\mathbf{Y}(\omega) = \left[\ldots \ \mathbf{y}_{-1}^{\mathrm{T}}(\omega) \ \ \mathbf{y}_0^{\mathrm{T}}(\omega) \ \ \mathbf{y}_1^{\mathrm{T}}(\omega) \ \ \ldots\right]^{\mathrm{T}}$, then the harmonic transfer function (HTF) can be established for the LPTV system. The HTF is completely analogous to the commonly known transfer function for LTI systems.

The harmonic transfer function is derived by inserting this modulated signal into the general solution in Eq. (3), and using the modal solution from in Eq. (7). The harmonic balance approach is taken to match the terms with the same frequency in the exponent $e^{(\mathrm{i}\omega + \mathrm{i}m\Omega)t}$. After much algebra and organization, a harmonic transfer function is obtained in terms of the modal parameters of the state transition matrix,

$$\mathbf{Y}(\omega) = \mathbf{G}(\omega)\mathbf{U}(\omega), \tag{12}$$

where $\mathbf{U}(\omega) = \left[\ldots \ \mathbf{u}_{-1}^{\mathrm{T}}(\omega) \ \ \mathbf{u}_0^{\mathrm{T}}(\omega) \ \ \mathbf{u}_1^{\mathrm{T}}(\omega) \ \ \ldots\right]^{\mathrm{T}}$ is the exponentially modulated input in the frequency domain. And,

$$\begin{aligned}
\mathbf{G}(\omega) &= \sum_{r=1}^{2N} \sum_{l=-\infty}^{\infty} \frac{\bar{\mathbf{c}}_{r,l} \bar{\mathbf{b}}_{r,l}}{\mathrm{i}\omega - (\lambda_r - \mathrm{i}l\omega_A)} \\
\bar{\mathbf{c}}_{r,l} &= \left[\ldots \ \ \bar{c}_{r,-1-l} \ \ \bar{c}_{r,-l} \ \ \bar{c}_{r,1-l} \ \ \cdots\right]^{\mathrm{T}} \\
\bar{\mathbf{b}}_{r,l} &= \left[\cdots \ \ \bar{b}_{r,l+1} \ \ \bar{b}_{r,l} \ \ \bar{b}_{r,l-1} \ \ \cdots\right]
\end{aligned} \tag{13}$$

The m^{th} term in the vector $\bar{\mathbf{c}}_{r,l}$ is $\bar{c}_{r,l}$, which is the $(m\text{-}l)^{\text{th}}$ Fourier coefficient (or vector of Fourier coefficients) of $\mathbf{C}(t)\boldsymbol{\psi}_r(t)$. Note that the mode vectors $\bar{\mathbf{c}}_{r,l}$ acquired at different peaks describe the same shape but the elements are shifted in position in each vector. For example, supposing the mode vector at frequency λ_r is $\bar{\mathbf{c}}_{r,0} = [0 \ a \ b \ c \ \ 0]^{\mathrm{T}}$, the mode vector at $\lambda_r + \Omega$ should be $\bar{\mathbf{c}}_{r,-1} = [a \ b \ c \ 0 \ 0]^{\mathrm{T}}$ multiplied with an unknown constant, and the mode vector at $\lambda_r - \Omega$ should be proportional to $\bar{\mathbf{c}}_{r,1} = [0 \ 0 \ a \ b \ c]^{\mathrm{T}}$. A least squares approach can be used to extract the best estimate of the mode vector $\bar{\mathbf{c}}_{r,l}$ from the multiple estimations. Similarly, $\bar{\mathbf{b}}_{r,l-m}$ is the $(l\text{-}m)^{\text{th}}$ Fourier coefficient of $\mathbf{L}_r(t)^{\mathrm{T}}\mathbf{B}(t)$.

2.3 Harmonic Power Spectrum

In practice one has presumably measured the response of an LPTV system to an excitation that satisfies OMA assumptions, and the measured responses are a collection of time histories recorded at N_o DOFs: $\mathbf{y}(t) \in \mathbb{R}^{N_o}$, sampled with sampling frequency F_S. These time histories are then exponentially modulated by multiplying by $e^{-\mathrm{i}m\Omega t}$, $m = -M \ldots M$ to obtain a collection of responses $\mathbf{y}_m(t) \in \mathbb{C}^{N_o(2M+1)}$ and hence the harmonic power spectrum (HPS) matrix found in the conventional manner as in the LTI case:

$$\mathbf{S}_{YY}(\omega) = \mathrm{E}\left(\mathbf{y}_m(\omega)\mathbf{y}_m(\omega)^{\mathrm{H}}\right), \tag{14}$$

where E() is the expectation, and $()^{\mathrm{H}}$ denotes the Hermitian transpose. Retaining only the dominant terms, the HPS can be written in the following form in terms of the modes of the LPTV system,

$$\mathbf{S}_{YY}(\omega) \approx \sum_{r=1}^{2N} \sum_{l=-\infty}^{\infty} \frac{\bar{\mathbf{c}}_{r,l} \mathbf{W}(\omega)_r \mathbf{c}_{r,l}^{\mathrm{H}}}{\left[\mathrm{i}\omega - (\lambda_r - \mathrm{i}l\Omega)\right]\left[\mathrm{i}\omega - (\lambda_r - \mathrm{i}l\Omega)\right]^{\mathrm{H}}} \tag{15}$$

The terms $(\lambda_r - il\,\Omega)$ cause the HPS to have a peak near the system's eigenvalues or Floquet exponents, λ_r, and also at the eigenvalue plus some integer multiple of the fundamental frequency l. Here $\mathbf{W}(\omega)_r$ is related to the auto-spectrum of modulated input signal. In output-only modal analysis of LTI systems, the input is assumed to be uncorrelated random white noise and the auto spectrum of input signal becomes constant. The same assumption is used for LPTV systems.

The HPS has the same modal summation form as the power spectrum of an LTI system,

$$\mathbf{S}_{YY}^{\mathrm{LTI}}(\omega)=\sum_{r=1}^{N}\frac{\boldsymbol{\varphi}_r S_{UU}^{\mathrm{LTI}}(\omega)\boldsymbol{\varphi}_r^{\mathrm{H}}}{\left[\mathrm{i}\omega-\lambda_r\right]\left[\mathrm{i}\omega-\lambda_r\right]^{\mathrm{H}}}\,. \tag{16}$$

This function produces a peak in the spectrum when the excitation frequency ω is near the natural frequency $\mathrm{Im}(\lambda_r)$, and the peak can be curve-fitted to identify the natural frequencies, damping ratios and mode shapes of the system. Hence, the same algorithms for LTI systems can be used to identify modal parameters of an LPTV system, and the same intuition that is used to interpret frequency response functions can also be used to interpret the harmonic transfer function. However, there are a few differences that must be noted in signal processing:

- An LPTV system theoretically has an infinite number of peaks for each mode. The peaks occur at the frequencies $\omega = \mathrm{Im}(\lambda_r - \mathrm{i}l\,\Omega)$. If the observed mode shapes $\mathbf{C}(t)\boldsymbol{\psi}_r(t)$ are constant in time, $\bar{\mathbf{c}}_{r,l}$ and $\bar{\mathbf{b}}_{r,l}$ contain only one nonzero term, i.e., $\bar{c}_{r,0}$ and $\bar{b}_{r,0}$. Then, Eq. (13) and Eq. (15) reduce to the familiar relationship for an LTI system.
- The mode vectors of an LTI system describe the spatial pattern of deformation of a mode. For an LPTV system, the vectors $\bar{\mathbf{c}}_{r,l}$ consist of the Fourier coefficients that describe the time periodic spatial deformation pattern.

2.4 Complex Time Series: Rigorous Approach

In the approach outlined above the measured signal $\mathbf{y}(t)$ is multiplied by $e^{-\mathrm{i}m\,\Omega\,t}$, which could also be written as $e^{-\mathrm{i}m\,\Omega\,t} = \cos(m\,\Omega\,t) - \mathrm{i}\sin(m\Omega t)$. Hence, one could obtain the same result by multiplying the signals by a sine and cosine to form the real and imaginary parts separately. Eq. (15) shows that the HPS is simply a sum of damped exponential terms. One can show that each term leads to an exponential term in the time domain of the form $\mathbf{A}_{r,l}e^{(\lambda_r-\mathrm{i}l\Omega)t}$.

The residue matrix at the l^{th} harmonic of the r^{th} mode is defined as follows:

$$\mathbf{A}_{r,l}=\frac{\bar{\mathbf{c}}_{r,l}\mathbf{W}(\omega)_r\bar{\mathbf{c}}_{r,l}^{H}}{\zeta_r\omega_r}\,. \tag{17}$$

Hence, if the signal is modulated with a real sine and cosine rather than with $e^{-\mathrm{i}m\,\Omega\,t}$, and the residues obtained are $\mathbf{A}_{r,l}^{\mathrm{S}}$ and $\mathbf{A}_{r,l}^{\mathrm{C}}$ for the sine and cosine cases respectively, then the desired residues should simply be

$$\mathbf{A}_{r,l}=\mathbf{A}_{r,l}^{\mathrm{C}}-\mathrm{i}\mathbf{A}_{r,l}^{\mathrm{S}}\,. \tag{18}$$

The disadvantage of this approach, is that the signals become twice as large (twice as many outputs) compared to the case where complex time series are allowed. Also note that the sine and cosine terms should be treated simultaneously in a global curve fitting algorithm, to assure that the residues obtained correspond to precisely the same poles.

2.5 Simplified approach

This algorithm takes a different approach, seeking to produce a time series that is real and yet has the same spectrum for all positive frequencies. To explain it, it is helpful to first recall that when using the conventional approach, one forms the HPS matrix $\mathbf{S}_{YY}(\omega)$ as (14), $\mathbf{S}_{YY}(\omega)\in\mathbb{C}^{N_o(2M+1)\times N_o(2M+1)}$. Then several rows of the matrix are selected, and peak-picking is used to determine modal parameters. It is important to note that for peak-picking one uses only the frequencies $0<\omega<\pi F_S - M\Omega$, i.e. those lying in the positive part of the frequency axis.

The presented study suggests replacing the frequency domain peak-picking method by more robust OMA-SSI algorithms, which are available in some commercial software packages (for example, Bruel and Kjaer

Type 7780). Thus, its combination with the exponential modulation will allow the traditional OMA-SSI to be readily applied to LPTV systems.

The problem, however, is that the commercial OMA-SSI does not accept complex time histories. In order to circumvent this limitation, the following is suggested: Assume there is a procedure that converts the exponentially modulated time histories $\mathbf{y}_m(t) \in \mathbb{C}$ to new time histories $\tilde{\mathbf{y}}_m(t)$ with the following properties:

$$\tilde{\mathbf{y}}_m^{(n)}(t) \in \mathbb{R} \tag{19}$$

$$\mathcal{F}(\tilde{\mathbf{y}}_m(t)) = \mathcal{F}(\mathbf{y}_m(t)) \text{ for } \omega \in [0, \pi F_S], \tag{20}$$

where $\mathcal{F}(..)$ denotes the Fourier transform. The first property ensures the new signals are usable in the available implementations of the SSI-OMA algorithms, while the second means that

$$\tilde{\mathbf{S}}_{YY}(\omega) = \mathbf{S}_{YY}(\omega) \text{ for } \omega \in [0, \pi F_S], \tag{21}$$

i.e. the new time histories $\tilde{\mathbf{y}}_m(t)$ have the same frequency content and phase relations as the positive half of the harmonic power spectra which is being utilized in the HPS method.

From properties (19) and (20), one can readily derive the algorithm converting $\mathbf{y}_m(t)$ to $\tilde{\mathbf{y}}_m(t)$:

1. For given exponentially modulated signals $\mathbf{y}_m(t)$ compute their periodogram $\mathcal{F}(\mathbf{y}_m(t))$ using a fast Fourier transform. The periodogram of complex $\mathbf{y}_m(t)$ is not a Hermitian function, i.e. its negative frequencies part is not a complex conjugate of the positive frequencies part;
2. Replace the negative frequencies part of the periodogram by the complex conjugate of the positive part;
3. Using inverse FFT, generate the new time signals $\tilde{\mathbf{y}}_m(t)$, which satisfy (19) and (20).

3 Results

To demonstrate the algorithm, let us consider a simple three-bladed rotor system, which is a rough model of a horizontal axis wind turbine (Figure 1). Each blade is modelled as a two-beams assembly; the beams are connected by a hinge with a linear angular spring with stiffness k_j, j=1...3, (here and below j is the blade index). A lumped mass m_j is attached to the end of the outer beam. The azimuth angles of the blades are: $\psi_j(t) = \Omega t + 2\pi(j-1)/3$, where the rotor angular speed Ω is assumed constant. The rotor is attached to the "nacelle" C with mass m_N supported by the "tower" modelled by two springs with stiffnesses k_H and k_V. The rotor is linked to the "drivetrain" with moment of inertia I_D and stiffness k_D.

For examination of the rotor modal behaviour, the following parameters were chosen, same as in [18]: $m_N = 446\ 10^3\ kg$, $m_1 = m_2 = m_3 = 41.7\ 10^3\ kg$, $k_1 = k_2 = k_3 = 2.006\ 10^8\ N \cdot m$, $k_D = 10^8\ N \cdot m$, $k_H = 2.6\ 10^6\ N/m$, $k_V = 5.2\ 10^8\ N/m$, $I_D = 2.6\ 10^7\ kg \cdot m^2$, $a = b = 13.1\ m$, $\Omega = 2\pi\ 0.16\ rad/s$. These parameters approximate a generic 10 MW wind turbine model.

The identical system was considered in [18], where the equations of motion were set up and the Floquet analysis was applied to investigate the influence of rotor's anisotropy to whirling components of the mode shapes.

Since this is a six degree-of-freedom system, one shall expect six modes, which are named as follows:

- the *vertical* and *horizontal* modes, dominated by vertical and horizontal motion of the mass C;
- three rotor modes: one symmetric (also called *collective*), where all blades deflect in-phase, and two anti-symmetric, also called *whirling*;
- a "*drivetrain*" mode, where the most of potential energy is being stored in the stiffness k_D.

One must not expect pure modes, there is always some degree of interaction; the names are only given to reflect the dominating motion of the mode. The presented study focuses on the rotor modes since they have the most pronounced periodic behavior.

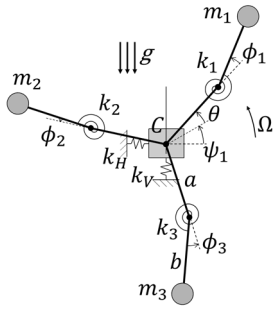

Figure 1. Considered system.

The presented study applies three methods to the system. First, we assume the equations of motion are known. This allows application of Floquet analysis and generates an (almost) exact solution; this solution serves as a baseline for comparison with two other methods. Next, we simulate an experimental scenario: we assume the equations of motion are unknown but we can observe the response of the system to excitation, which satisfies OMA assumptions: all DOFs are excited by uncorrelated broadband noise with a flat spectrum. Then both the conventional frequency domain HPS method and the suggested time-domain method are applied to the observed response, and the results are compared.

3.1 Floquet analysis

An overview and a detailed description of Floquet analysis can be found e.g. in [19]. Floquet analysis was applied to the system in Figure 1; the details are given in [18] and omitted here. As was mentioned in the theoretical section, Floquet analysis provides a modal decomposition, but for an LPTV system, the modes are periodic. Following the conventional approach, each periodic mode is Fourier expanded to harmonic (Fourier) components. The LTI system can then be thought as a special case of LPTV, where each mode has only one non-zero Fourier component. It can be shown that for an isotropic three-bladed rotor in the absence of gravity, each mode has three non-zero Fourier components. The Coleman transformation [20] utilizes this phenomena and allows conversion of the LPTV system to LTI system. A stronger periodicity of the system matrix in Eq. (1) requires more Fourier components to be included into consideration. For almost isotropic rotors, only few Fourier components have significant magnitude, and the smaller components can be neglected.

Figure 6a,c shows the magnitudes of the harmonic components obtained via Floquet analysis for isotropic rotor in the absence of gravity. Two modes are shown: forward whirling (FW) mode (which is dominated by x_C but named after its significant whirling component), and collective mode. The backward whirling (BW) is explained in details in Figure 7. As it was mentioned before, the modes of a (three-bladed) isotropic rotor in the absence of gravity can be fully described by only three Fourier components.

Figure 7 focuses on the BW mode. Figure 7c shows the magnitude of its three non-zero Fourier components: FW component (A), motion of the center mass (B) and BW component (C). The latter is about one order of magnitude higher than the FW component, it dominates the rotor dynamics, and the mode is named after this component. Figure 7a is a complexity plot showing the phase relation between the three blades. The left plot is for the FW component (A), where the phase between the consecutive blades is $+120^0$. The right plot is for the dominating BW component (C) with -120^0 phase.

Figure 8a,c,f shows the BW, FW and collective modes for anisotropic rotor in the presence of gravity. Compared to the isotropic rotor, the system matrix of the anisotropic rotor demonstrates higher and more complex variation with time, and, as a result, it requires more Fourier components to describe the periodic mode shapes (*cf.* Figure 6a,c and Figure 7b).

Table 2 provides the values of the Floquet exponents for both isotropic and anisotropic rotors.

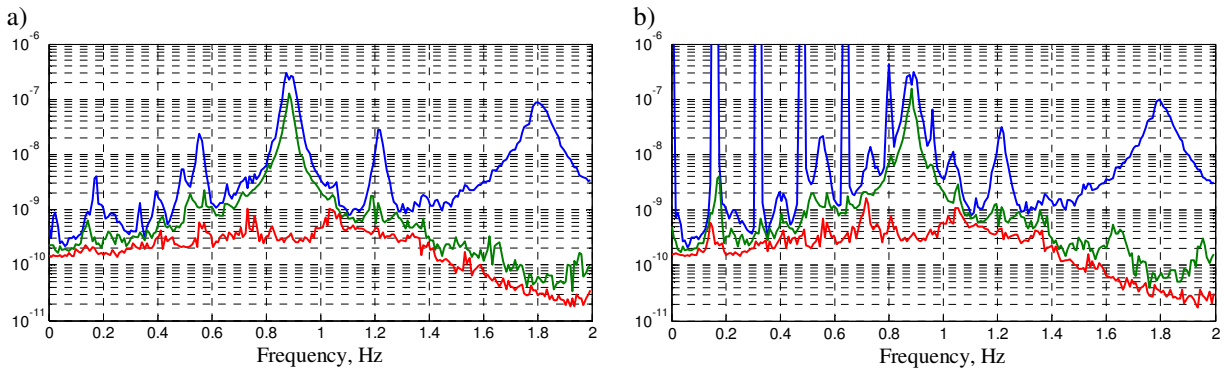

Figure 2. Complex Mode Indicator Function of the HPS Matrix for the 5 outputs using ϕ_1, ϕ_2, ϕ_3 as references. a) Isotropic rotor without gravity; b) Anisotropic rotor with gravity and k_C = 0.97.

3.2 Numerical experiment

As an input to the numerical experiment, we simulated the response of the rotor to uncorrelated broadband excitation. This excitation satisfies OMA assumptions, but we acknowledge that the aeroelastic forces acting on the wind turbine rotor in reality are different [21]. The equations of motion were numerically integrated using 4th order Runge-Kutta method, for 7200s (which correspond to 1152 rotor revolutions).

3.2.1 Results from H-OMA-FD

The simulated turbine rotates at 0.16Hz. The responses in the edgewise direction on all three blades (ϕ_1, ϕ_2, ϕ_3) and the responses of the nacelle in the lateral (X_c) and vertical (Y_c) directions were collected into a response vector of 5 outputs. The responses were then exponentially modulated with m= −3…3 according to Eq. (11). Then, the modulated signals were split into 575 sub-blocks with a block size of 119s (19 revolutions) with 85% overlap. A Hanning window was applied to each block to reduce the leakage. The cross power spectra between the modulated signals and the original signals ϕ_1, ϕ_2, ϕ_3 were computed respectively in each sub-block and averaged over the whole time history. The resulting harmonic power spectrum matrix had 35 outputs (5 outputs with 7 harmonics for each output) by 3 references. The complex mode indicator function (CMIF) of this HPS matrix is shown in Figure 2 for two cases, (a) isotropic rotor with no gravity, and (b) anisotropic rotor with k_C=0.97 and with gravity. There are two dominant singular values peaks in the CMIF, with very close natural frequencies centered around 0.88Hz. All of the other peaks except for the peak at 1.8 Hz were spaced by n×0.16 Hz from the peaks at 0.88 Hz, indicating that the system has three modes dominating this frequency range, and two of which have noticeable periodic behavior.

Initially, a simple output-only extension of the Algorithm of Mode Isolation (AMI) algorithm that was used to curve fit the measurements. This gave a reasonable fit at all of the peaks, but this algorithm does not

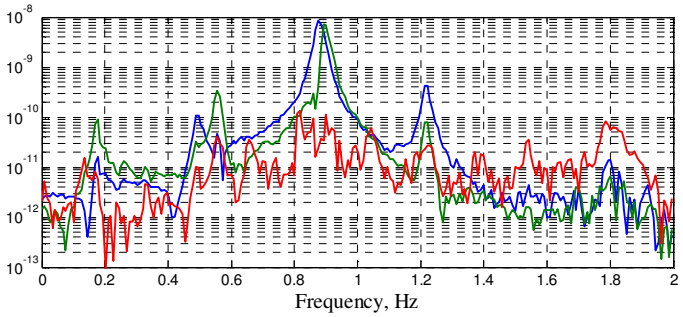

Figure 3. Spatially condensed MIMO measurements.

include the MIMO, hybrid approach described in [22, 23] which is necessary to separate modes with close natural frequencies. Hence, the only mode retained from AMI was the mode at 1.801 Hz, which was found to be the first collective mode of the rotor. The two close modes were estimated using frequency domain decomposition (FDD) [24]. Specifically, the spectra near the peak were collected and an SVD used to extract the first three dominant singular vectors. These were then used to condense the measurements to a set of three spectra, shown in Figure 3. This spatial condensation of the measurements effectively separated the two close modes, so that a simple single-mode fit could be applied to each curve to estimate the modal parameters. The natural frequencies and damping for the three rotor modes are given in Table 2. The magnitude of the Fourier components are shown in Figure 10a,c.

The next case considered is the case with gravity and with 3% anisotropy in one of the blades. Again, AMI identified the collective mode at 1.79 Hz, while the FDD was used to identify the other two modes. The modal parameters obtained are given in Table 2, and the mode shapes are in Figure 10e,g.

These results illustrate what can be done with a basic system identification method based on the HPS, and focus on the time-periodic blade modes. More sophisticated frequency-domain methods would be advisable to use, such as the AFPoly algorithm [25] or pLSCF [26].

3.2.2 Results from H-OMA-TD

The obtained response time histories became an input to the H-OMA-TD algorithm. Figure 4 sketches how the method is applied using B&K OMA software Type 7760. First, the dataset of time histories for all six DOFs obtained from the simulation (or from measurements) is harmonically modulated (using $m = -3..+3$ in the present study), thus generating six new datasets. The new (complex) time histories are converted to real time using the algorithm described in section 2.2. In OMA software, we construct 6 copies of the rotor geometry and assign the modulated datasets to the copies (Figure 4). The not modulated signals (m=0) are selected as projection channels (shown in pink). Then a standard OMA procedure is run (in the presented study, we used data driven OMA-SSI with un-weighted principal components, UPC), which extracts the modes.

A CMIF and the fragment of the stabilization diagram for the isotropic rotor in the absence of gravity are shown in Figure 5. In the range 0-1.5 Hz, OMA finds nine modes, however they are ±Ω shifted realizations of the three structural periodic modes: Horizontal, BW and FW. This can be clearly seen when examining the mode shapes: those corresponding to the BW mode are shown in the insets.

Table 1 explains the interpretation of the mode shapes using the BW mode as an example. The rows in the table corresponds to the modes found by OMA-SSI (see Figure 5). Examining the middle row BW n=0, one can realize that the periodic mode consists of three Fourier components *oscillating at different frequencies*: the horizontal component at 0.72Hz, backward whirling component at 0.88Hz and very weak forward

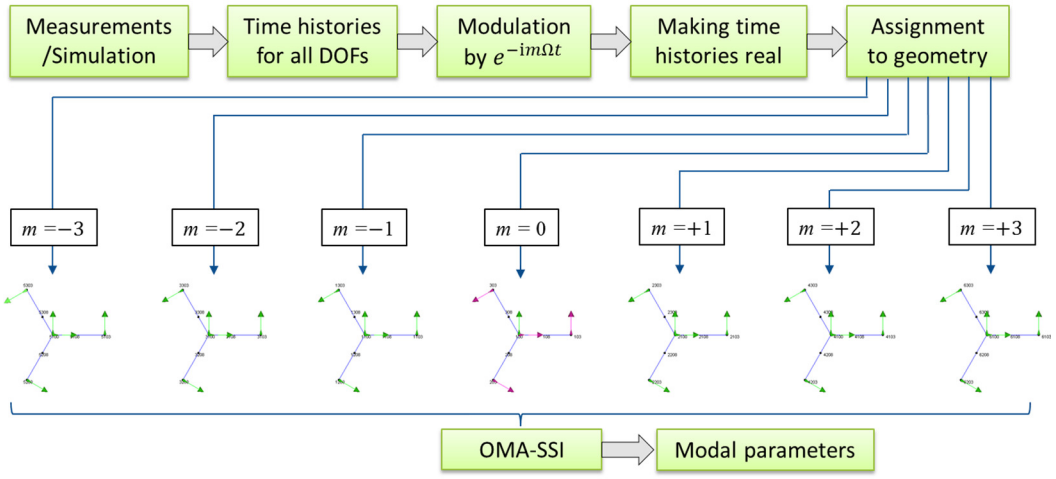

Figure 4. Flow of the suggested method

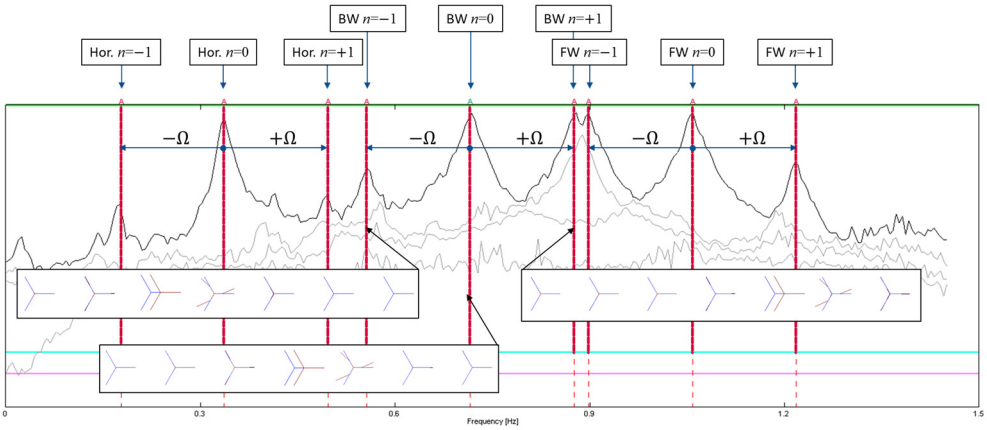

Figure 5. Fragment of the stabilization diagram (B&K Type 7760 OMA software) showing horizontal, BW and FW modes of the isotropic rotor with no gravity.

whirling component at 0.56Hz. While inspecting the top and bottom rows, one finds the same components at the same frequencies.

Note that the phase relations between DOFs are only valid inside each Fourier component and do not make sense between the components.

The values of the Fourier exponents are given in Table 2 and the magnitude of the Fourier components are shown in Figure 6bd and Figure 7d,e,f and compared with the results of analytical Floquet analysis. Both frequencies, damping and mode shapes are in a quite good agreement with the analytical values.

Figure 7 explains the results of H-OMA-TD in details using the BW mode as an example. The simulation was conducted for five different realizations of the excitation input, and the system identification was performed for each realization. Figures 7b,d,f show the mean magnitudes of the obtained Fourier components; the confidence bounds on the results based on the five observations are also shown. Though the H-OMA-TD algorithm produces many Fourier components, it can be seen that the confidence of the noise components is significantly lower (the confidence band is wider), and the false ones can be readily identified and filtered out. The true ones are shown inside the dotted region (Figure 7b,d,f), and coincide

Name	Frequency, Hz	Mode shape						
		m=−3	*m*=−2	*m*=−1	*m*=0	*m*=+1	*m*=+2	*m*=+3
BW *n*=−1	0.56	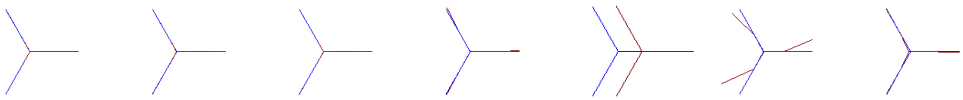						
		0.56−3Ω= 0.08Hz	0.56−2Ω= 0.24Hz	0.56−Ω= 0.40Hz	**0.56Hz**	0.56+Ω= **0.72Hz**	0.56+2Ω= **0.88Hz**	0.56+3Ω= 1.04Hz
BW *n*=0	0.72	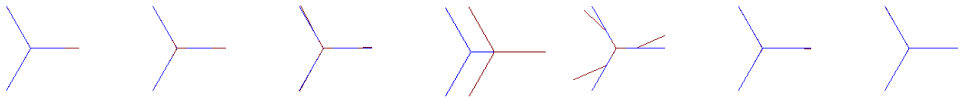						
		0.72−3Ω= 0.24Hz	0.72−2Ω= 0.40Hz	0.72−Ω= **0.56Hz**	**0.72Hz**	0.72+Ω= **0.88Hz**	0.72+2Ω= 1.04Hz	0.72+3Ω= 1.20Hz
BW *n*=+1	0.88	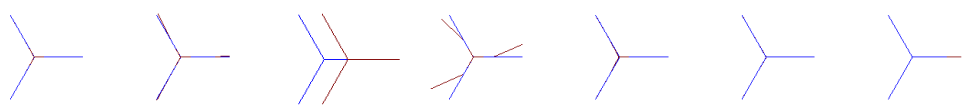						
		0.88−3Ω= 0.40Hz	0.88−2Ω= **0.56Hz**	0.88−Ω= **0.72Hz**	**0.88Hz**	0.88+Ω= 1.04Hz	0.88+2Ω= 1.20Hz	0.88+3Ω= 1.36Hz

Table 1. Isotropic rotor with no gravity. Shapes of the Fourier components for BW mode for different *n*.

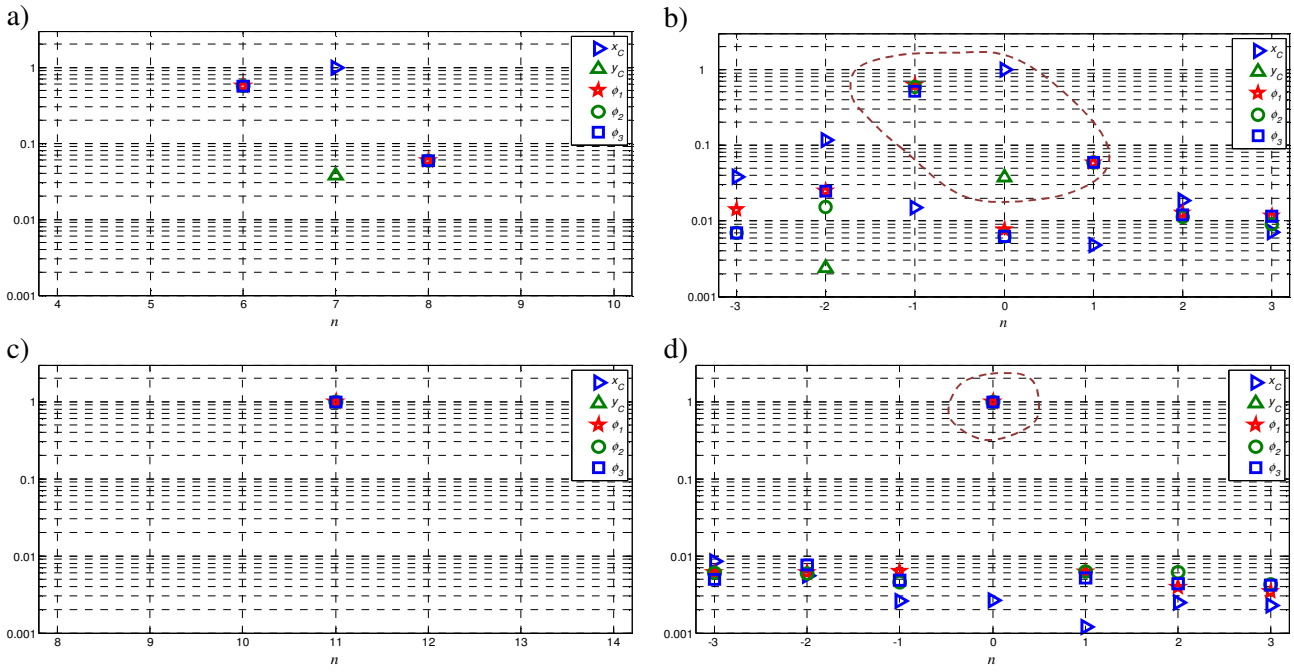

Figure 6. Isotropic rotor with no gravity. (a,b): FW mode; (c,d): collective mode. (a,c): Results of the Floquet analysis; (b,d): Results of H-OMA-TD for the simulated experiment.

with the analytical results obtained via Floquet analysis. Figure 7e shows the scatter of the shape of the BW and FW Fourier components (*cf.* analytical plots in Figure 7a).

Figure 8 compares the results of Floquet analysis with the results of H-OMA-TD for anisotropic rotor in the presence of gravity. The dashed lines surround the regions where the H-OMA-TD methods catches the Fourier components pretty well. These components dominate the dynamics of the mode, while the others are significantly lower in magnitude. The dotted line in Figure 8b shows the erroneous components which do not present in the analytical solution (Figure 8a). These components can be explained by the strong influence of the rotor harmonics present nearby the component frequencies (see the strong peaks in Figure 2b). Table 2 provides the Floquet exponents and compares them with the analytically ones; both agree quite well.

The complexity plots in Figure 9 compare the dominating Fourier components for the two whirling modes. The rotor anisotropy causes the asymmetry of the shapes. Despite the scatter, this observed asymmetry can be used as an indicator of a damage (here, the stiffness of blade #3 is reduced by 3%). This may also be used to localize the damage [18].

3.2.3 Result comparison

Table 2 provides Floquet exponents obtained analytically and compares them with the frequencies found by time- and frequency domain H-OMA methods. Regarding damping, one can notice that, if it is defined with a damping ratio, then it depends on chosen the natural frequency. The latter is not invariant since a shift by an integer multiplier of Ω is also a natural frequency (e.g. Table 1). However, the real part of the Floquet multipliers is invariant, and can be used to characterize the damping and system stability.
Figure 10 compares the magnitudes of modal components of BW and FW modes obtained by frequency and time domain methods for the isotropic rotor in the absence of gravity (Figure 10a-d) and anisotropic rotor when the gravity is present (Figure 10e-h). The dominant components of the modes are outlined by a dashed line. As one can observe, the two methods provide similar results, though the frequency domain method gets slightly wrong results reporting the different magnitudes of ϕ_1, ϕ_2, ϕ_3 for the isotropic case (outlined by the dotted lines). This might be possibly improved by using a multi-reference technique. The same can be

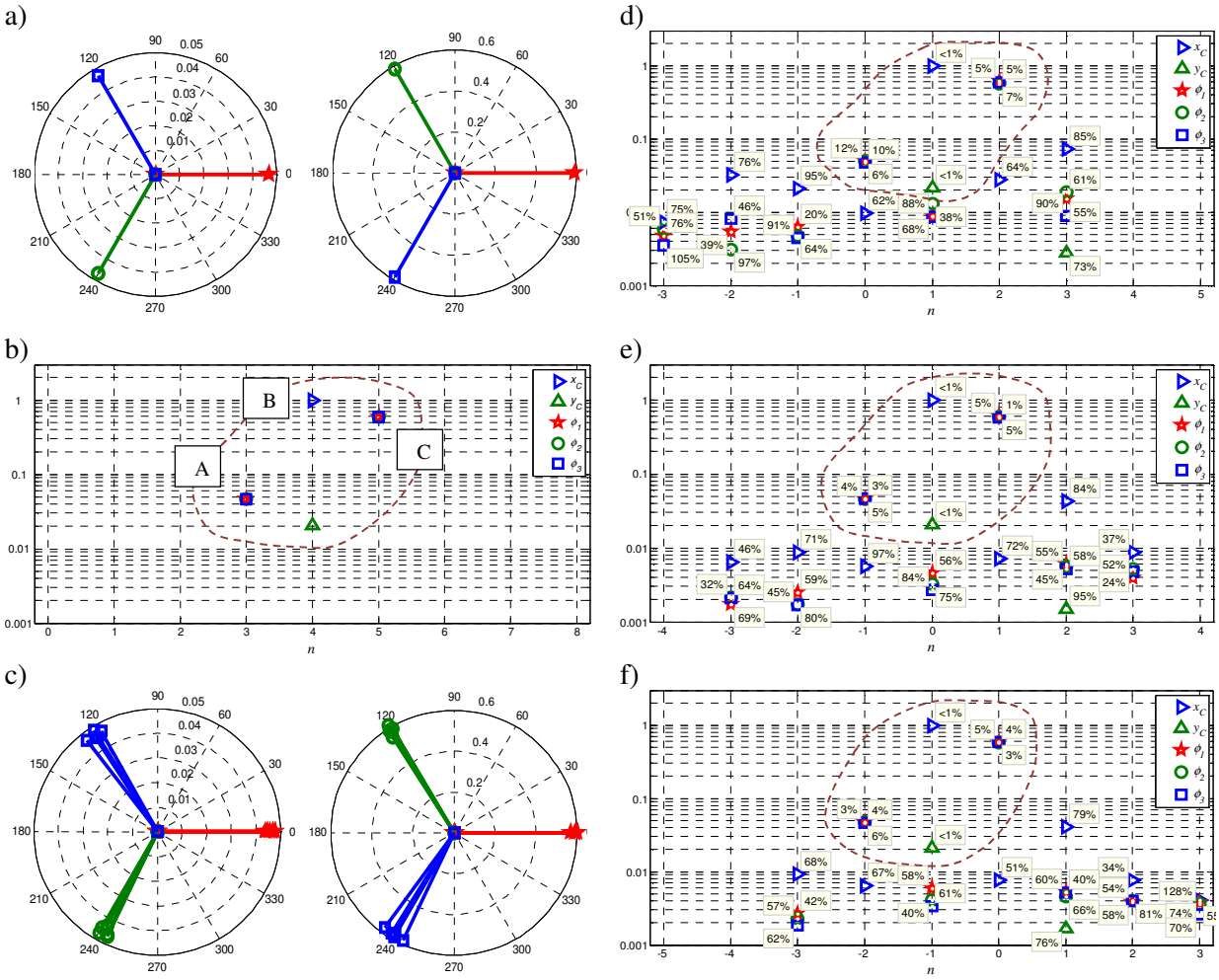

Figure 7. The BW mode of isotropic rotor with no gravity. a) Shapes of the FW (left) and BW (right) components (via Floquet analysis); b) Magnitude of Fourier components (via Floquet analysis); c) Same as (a) via H-OMA-TD; d-f) Magnitudes of Fourier components for: d) $n = -1$, e) $n = 0$, f) $n = +1$, as in Table 1. The per-cent values in the boxes are a half-width of the pointwise 95% confidence bands computed based on five analysis, using Student's t-distribution.

said regarding the phase. The natural frequencies reported by the two methods differ by Ω, which is natural for periodic systems. Actually, the mode shown in Figure 10a is fully comparable with the representation "BW n=+1" found in Table 1.

It is also interesting to compare the results of H-OMA-TD with the results of *direct* application of OMA to the measured data, thus ignoring the fact that the system is LPTV. This approach was used for example, in [18]. In the framework of the H-OMA-TD method, it means narrowing the range of m in (11) to 0. As it follows from Table 1, it will still be possible to extract the Fourier components (each found mode will be a Fourier component). If the LPTV nature of the system is recognized, one has to manually assemble the mode from the found Fourier components, knowing that they are separated by integer multipliers of Ω. It is also important to note that the mutual scaling of the Fourier components will be lost in this case.

4 Conclusion and future research

The study suggests a simple method of extending existing implementations of time domain OMA SSI algorithms to time periodic systems. The method consists of two steps: (i) harmonic modulation of the experimentally obtained time histories (by multiplication by $e^{-\mathrm{i}m\Omega t}$); (ii) making the obtained complex

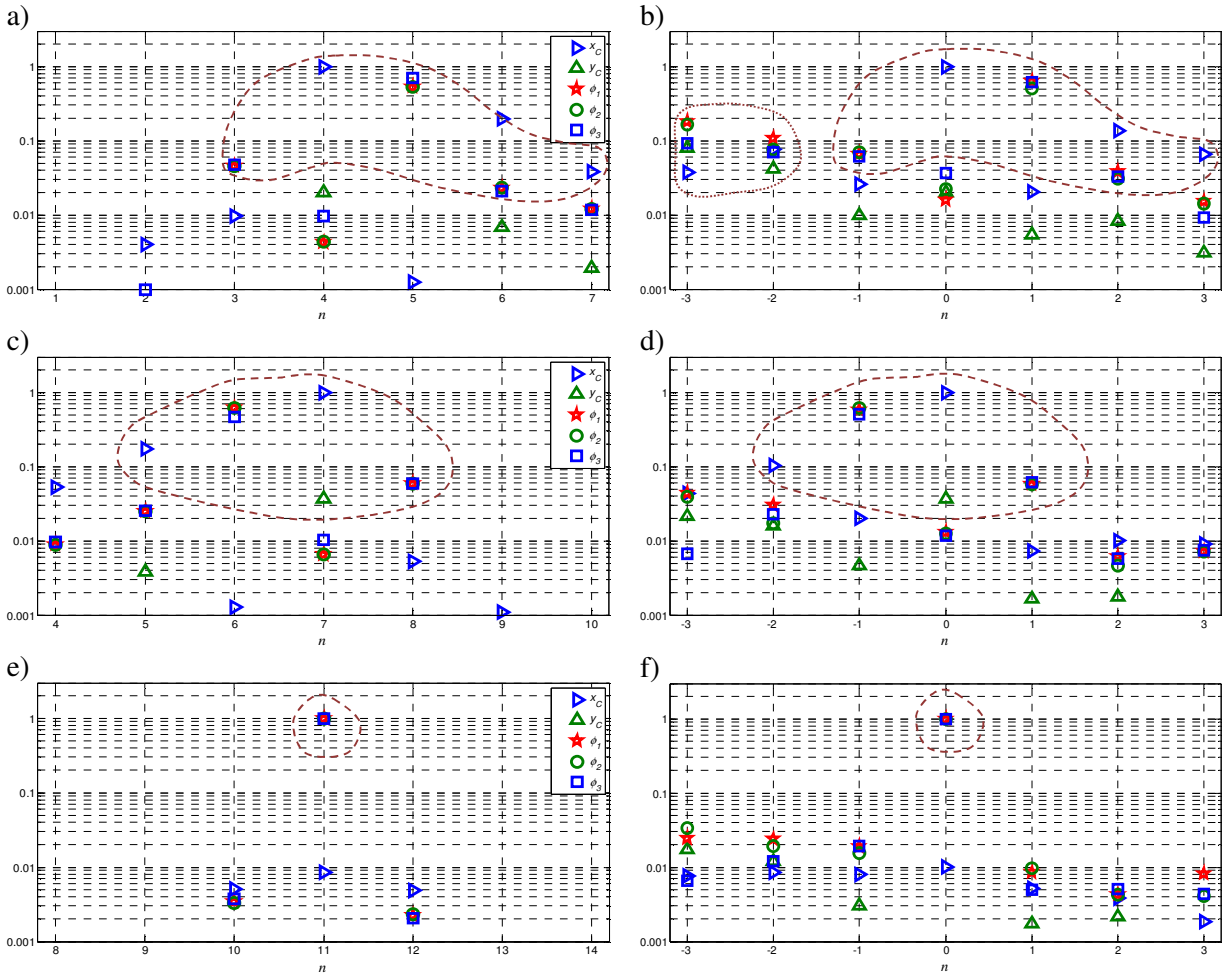

Figure 8. Magnitudes of the Fourier components for anisotropic rotor: BW (top row), FW (middle row) and collective (bottom). Left column: results of the Floquet analysis; right column: H-OMA-TD for simulated experiment. Dashed lines show the significant components, dotted line shows the erroneous results due to vicinity to strong rotor harmonics.

time histories real. The preprocessed data becomes an input to standard OMA algorithm. In addition, the authors give some advice on how to prepare the data for OMA, to more easily interpret the results.

The method is demonstrated on synthesized data obtained via simulation of a simple 3-bladed rotor subjected to random noise excitation. The results of this simulated experiment are validated against the analytical results from Floquet analysis and the results provided by the conventional HPS method implemented in the frequency domain. The suggested algorithm avoids the manual peak picking and allows automation, which could be useful, for example, in structure health monitoring systems.

The suggested method is originated from engineering practice, and requires a better mathematical foundation. Mode shape normalization and scaling when using acceleration measurements and estimation of damping ratio need to be addressed. Application of the method to real measurements from a wind turbine would be a natural next step.

Acknowledgements

The work is partly supported by EUDP (Danish Energy Technology Development and Demonstration Programme), grant number 64011-0084 “Predictive Structure Health monitoring of Wind Turbines”.

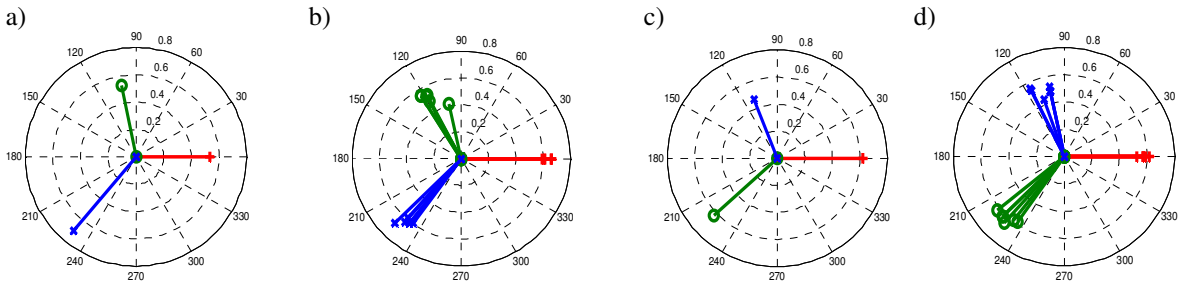

Figure 9. Complexity plots: anisotropic rotor. Blade #3 has a 3% reduction in stiffness. a) BW mode, the BW (dominating) component, exact solution; b) same, the H-OMA-TD results for five simulated experiments; c) FW mode, the FW (dominating) component, exact solution, d) same, the H-OMA-TD results for five experiments.

Mode Name	Floquet exponent $\lambda/(2\pi)$	n	Un-aliased Floquet exponent $(\lambda + n\,\Omega)/(2\pi)$	H-OMA-TD (n=0) (in Hz)	H-OMA-FD (in Hz)
Isotropic rotor, no gravity					
BW	−0.0112 + 0.0764i	4	−0.0112 + 0.7164i	−0.0116(±0.0013) + 0.7162(±0.0008)i	−0.0140+ 0.7159i
FW	−0.0117 - 0.0610i	7	−0.0117 − 1.0590i	−0.0113(±0.0007) + 1.0587(±0.0025)i	−0.0102+ 1.0540i
Collective	−0.0348 + 0.0464i	11	−0.0348 + 1.8064i	−0.0353(±0.0014) + 1.8064(±0.0032)i	−0.0360+ 1.8006
Anisotropic rotor, with gravity					
BW	−0.0111 + 0.0716i	4	−0.0111 + 0.7116i	−0.0122(±0.0018) + 0.7121(±0.0006)i	−0.0118+ 0.7129i
FW	−0.0116 − 0.0648i	7	−0.0116 − 1.0552i	−0.0113(±0.0008) + 1.0547(±0.0011)i	−0.0105+ 1.0549i
Collective	−0.0345 + 0.0378i	11	−0.0345 + 1.7985i	−0.0353(±0.0019) + 1.7985(±0.0032)i	−0.0286+ 1.7858i

Table 2. Floquet exponents obtained analytically, by H-OMA-TD and H-OMA-FD.

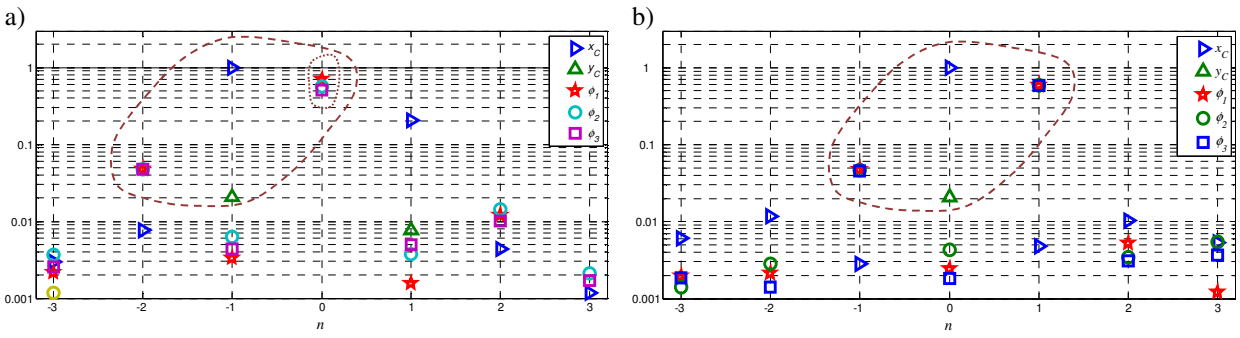

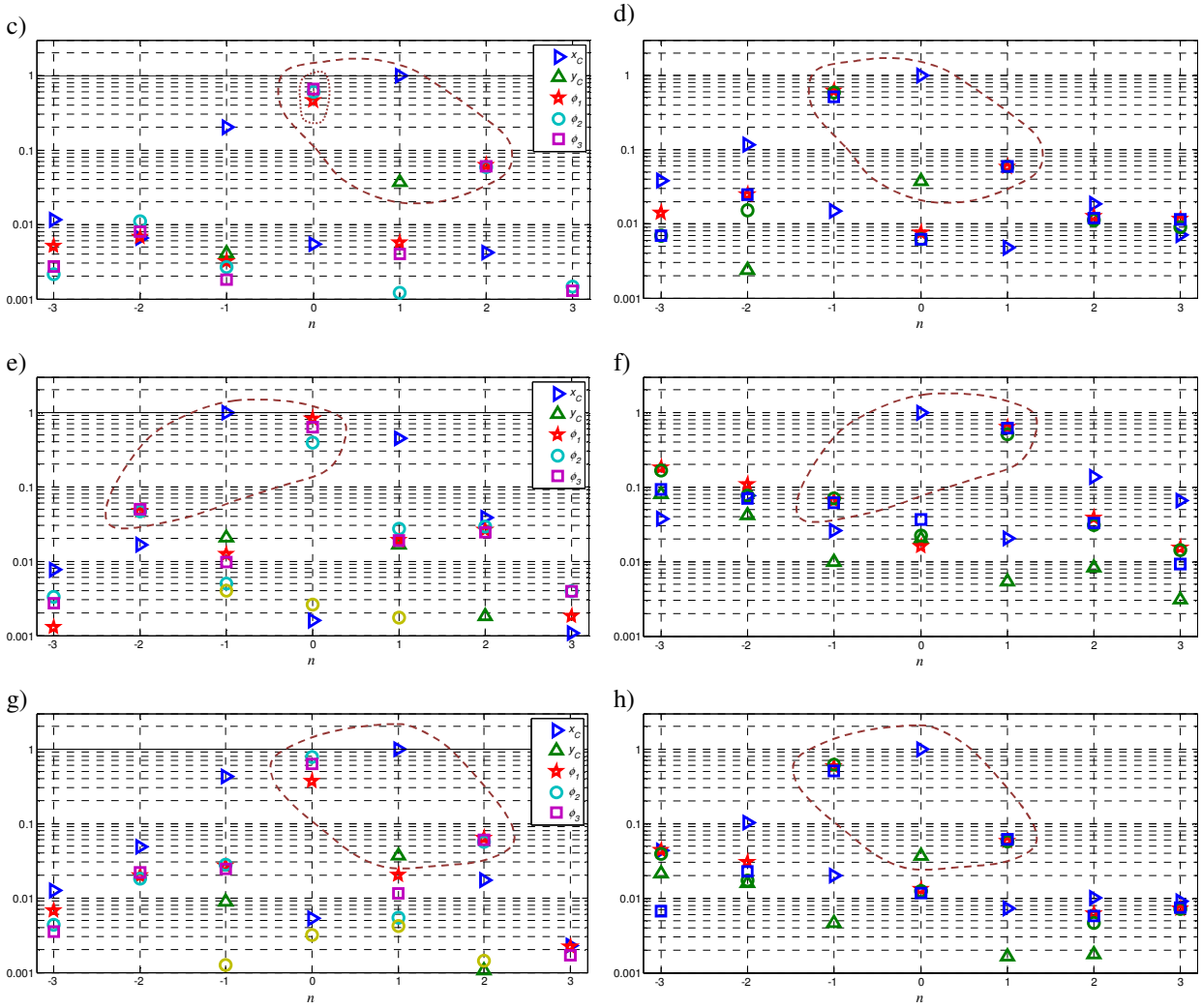

Figure 10.Magnitudes of modal components obtained by H-OMA-FD (left column) and H-OMA-TD (right column). a,b) Isotropic rotor in the absence of gravity, BW mode; c,d) same, FW mode; e,f) anisotropic rotor in the presence of gravity, BW mode; g,h) same, FW mode.

References

[1] G. H. James, T. G. Carne, *Damping measurements on operating wind turbines using the natural excitation technique (NExT)*. In *Proceedings of 11th ASME Wind Energy Symposium presented at the Energy Sources Technology Conference and Exhibition*. Houston, USA (1992). Vol. 12, pp. 75-81.

[2] D. Tcherniak, S. Chauhan, M. Rossetti, I. Font, J. Basurko, O. Salgado. *Output-only Modal Analysis on Operating Wind Turbines: Application to Simulated Data*. In: *Proceedings of European Wind Energy Conference*, Warsaw, Poland (2010).

[3] A. Jhinaoui, *Subspace-based identication and vibration monitoring algorithms for rotating systems*, PhD Thesis, Rennes, France (2014).

[4] M.S. Allen, *Frequency-Domain Identification of Linear Time-Periodic Systems using LTI Techniques*, Journal of Computational and Nonlinear Dynamics, Vol. 4, No. 4 (2009).

[5] M.S. Allen, M. W. Sracic, et al. *Output-Only Modal Analysis of Linear Time Periodic Systems with Application to Wind Turbine Simulation Data*, Mechanical Systems and Signal Processing Vol. 25 (2011), pp. 1174-1191.

[6] S. Yang, M. S. Allen, *A Lifting Algorithm for Output-only Continuous Scan Laser Doppler Vibrometry*, In *Proceedings of 53rd AIAA Structures, Structural Dynamics, and Materials Conference*. Honolulu, Hawaii (2012).
[7] S. Yang, M. S. Allen, *Output-Only Modal Analysis Using Continuous-Scan Laser Doppler Vibrometry and Application to a 20kW Wind Turbine*, Mechanical Systems and Signal Processing Vol.31 (2012), pp. 228–245.
[8] S. Yang, M. S. Allen, *Transfer Functions to Measure Translational and Rotational Velocities with Continuous-Scan Laser Doppler Vibrometry*, In *Proceeding of 31st International Modal Analysis Conference (IMAC XXXI),* Garden Grove, CA, USA (2013).
[9] S. Yang, M. S. Allen, *Harmonic Transfer Function to Measure Translational and Rotational Velocities With Continuous-Scan Laser Doppler Vibrometry*, Journal of Vibration and Acoustics, Vol. 136, No. 2, (2014).
[10] S. Yang, S., D. Tcherniak, M. S. Allen, *Modal Analysis of Rotating Wind Turbine using Multi-blade Coordinate Transformation and Harmonic power spectrum*, In *Proceedings of 32nd International Modal Analysis Conference (IMAC XXXII)*, Orlando, FL, USA (2014).
[11] J. H. Ginsberg, *Mechanical and Structural Vibrations*. New York, John Wiley and Sons (2001).
[12] C. Chen, *Linear Systems Theory and Design*. New York, Oxford University Press, Inc. (1999).
[13] N. M. Wereley, *Analysis and Control of Linear Periodically Time Varying Systems*, PhD Thesis, Massachusetts Institute of Technology, (1991).
[14] G. Floquet, *Sur Les Equations Lineairs a Coefficients Periodiques*, Ann. Sci. Ecole Norm. Sup., Vol. 12, (1883) pp. 47-88.
[15] P. Hartman, *Ordinary Differential Equations*, New York, John Wiley & Sons, Inc. (1964).
[16] J. Guckenheimer, P. Holmes, *Nonlinear Oscillations, Dynamical Systems, and Bifurcations of Vector Fields*. New York, Springer-Verlag New York Inc. (1983).
[17] H. Hochstadt, *Differential Equations*. New York, Dover (1964).
[18] D. Tcherniak, *Loss of Rotor Isotropy as a Blade Damage Indicator for Wind Turbine Structure Health Monitoring Systems*, In *Proceedings of European Workshop on Structure Health Monitoring (EWSHM)*, Nantes, France (2014).
[19] P. F. Skjoldan, *Aeroelastic modal dynamics of wind turbines including anisotropic effects*, PhD Thesis, Roskilde, Denmark (2011).
[20] M. H. Hansen, *Improved Modal Dynamics of Wind Turbines to Avoid Stall-induced Vibrations*. Wind Energy Vol. 6 (2003), pp.179-195
[21] D. Tcherniak, S. Chauhan, M. N. Hansen, *Applicability Limits of Operational Modal Analysis to Operational Wind Turbines*. In *Proceedings of 28th Int. Modal Analysis Conference (IMAC)*, Orlando, FL, USA (2010).
[22] M.S. Allen, *Global and Multi-Input-Multi-Output (MIMO) Extensions of the Algorithm of Mode Isolation (AMI)*, Doctorate, Georgia Institute of Technology (2005).
[23] M. S. Allen, J. H. Ginsberg, *Global, Hybrid, MIMO Implementation of the Algorithm of Mode Isolation*. In *Proceedings of 23rd International Modal Analysis Conference (IMAC XXIII)*. Orlando, FL, USA (2005).
[24] R. J. Allemang, D. L. Brown, *A Unified Matrix Polynomial Approach to Modal Identification*, Journal of Sound and Vibration Vol. 211, No. 3 (1998), pp. 301-322.
[25] H. Vold, K. Napolitano, et al, *Aliasing in modal parameter estimation: An historical look and new innovations*. In *Proceedings of 25th International Modal Analysis Conference*. Orlando, FL, USA (2007).
[26] P. P. Guillaume, P. Verboven, et al., *A Poly-Reference Implementation of the Least-Squares Complex Frequency-Domain Estimator*. In *Proccedings of International Modal Analysis Conference (IMAC XXI)*, Kissimmee, FL, USA (2003).